Solar water splitting for hydrogen production with Fe₂O₃ nanotubes prepared by anodizing method: effect of anodizing time on performance of Fe₂O₃ nanotube arrays

**Mohamad Mohsen Momeni · Yousef Ghayeb · Faezeh Mohammadi**

Abstract Self-organized iron oxide nanotubes were successfully prepared on the iron foils by a simple electrochemical anodization method in NH_4F organic electrolyte. The Fe_2O_3 nanotubes were characterized by field-emission scanning electron microscopy, energy dispersive X-ray spectroscopy, UV–vis absorbance spectra, and X-ray diffraction spectroscopy. Scanning electron microscopy images show that dependent upon the anodizing time, the pore diameters range from 30 to 45 nm. Crystallization and structural retention of the synthesized structure are achieved upon annealing the initial amorphous sample in oxygen atmosphere at 450 °C for 1 h. The crystallized nanoporous film, having a 2.04 eV bandgap, exhibited a maximum photocurrent density of 0.68 mA cm^{-2} in 1 M NaOH at 0.5 V versus Ag/AgCl. The current potential characteristics showed that the water-splitting photocurrent strongly depends on the anodizing time and its increases with anodization time.

1 Introduction

Photo-electrochemical (PEC) water splitting is an efficient and environmentally-friendly method to produce hydrogen from water using solar light. Solar energy driven water splitting combines several attractive features for energy utilization. The reactants and products are clean, and the process can be efficient. A typical PEC cell contains a working photo-anode that absorbs light to oxidize water and produce gaseous oxygen, protons, and photo-excited electrons.

$$2H_2O\,(l) + h\upsilon \rightarrow O_2(g) + 4H^+ + 4e^- \tag{1}$$
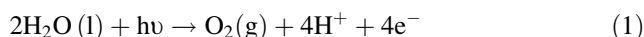
The formed photoelectrons (e^-) are sent to a counter cathode (usually made of a metal) via an external circuit. In the cathode, gaseous hydrogen is produced to complete overall water splitting.

$$2H^+ + 2e^- \rightarrow H_2(g) \tag{2}$$
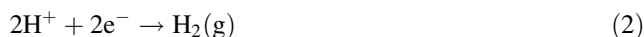
A schematic drawing of a typical PEC cell is shown in Fig. 1. The fabrication of the photo-electrode materials is the key to the successful construction of a high efficiency PEC cell. Since Fujishima and Honda first reported TiO_2 as photo-anode for the photo-electrolysis of water, the TiO_2 materials have been widely researched for photo-catalytic application [1]. Whereas, the wide band gap (3.2 eV) of TiO_2 material limits its practical application because it only can be excited with light of wavelength near or shorter than 385 nm. Other metal oxide semiconductors such as WO_3, ZnO, $BiVO_4$ and so have been extensively studied for photo-electrochemical water splitting [2–8]. However, because of the difficulty in discovering a single semiconductor that is capable of splitting water into hydrogen and oxygen, efforts to develop and optimize semiconductors for independent water oxidation and reduction are more realistic [9]. The primary scientific and technological objective has been focused on exploring novel photo-catalysts with high efficiency of utilization of solar irradiation, narrow band gap, operational stability and preparation with relatively low cost. Iron oxide, usually α-Fe_2O_3 (or hematite), has been studied extensively as a semiconductor photoanode material because of its narrow band gap (2.1 eV) that allows absorption of a large fraction (ca. 13.5 %) of solar light, stability in alkaline solutions, low cost, and ample

M. M. Momeni (✉) · Y. Ghayeb · F. Mohammadi
Department of Chemistry, Isfahan University of Technology, Isfahan 84156-83111, Iran
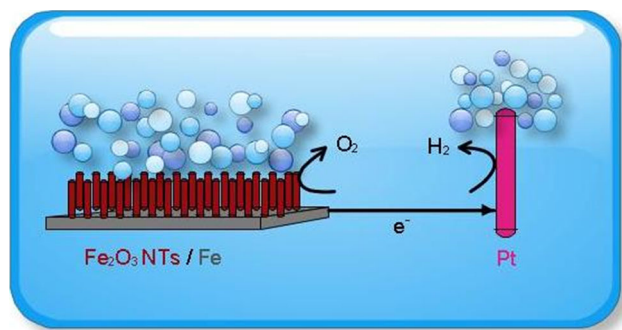e-mail: mm.momeni@cc.iut.ac.ir

Fig. 1 Schematic of a photo-electrochemical (PEC) cell, employing Fe_2O_3 nanotubes/Fe in the anode

abundance; furthermore, it is non-toxic and environmentally friendly [10–14]. However, the practical use of this material is limited because of its low electron mobility (10^{-2} to 10^{-1} cm^2 V^{-1} s^{-1}) and short hole diffusion length (2–4 nm), as well as the short life time of its charge carriers (about 10 pico second) that lead in practice to very low solar light to current conversion efficiencies and large over-potential for O_2 evolution [15]. Various strategies have been employed to address these issues, for example, doping of the material to adjust the carrier mobility, incorporation of co-catalysts which reduce the over-potential, surface passivation to minimize losses by carrier recombination at the semiconductor-electrolyte interface and so on [15–18]. Recently, nanostructuring techniques have been proven useful in increasing the performance of iron oxide for photo-response. The aligned nanotube has been considered the most suitable way to achieve larger enhancement of surface area without an increase of the geometric area, reduced the scattering of free electrons, and enhanced the electrons mobility, which could be expected to achieve higher photo-catalytic (PC) activities [19]. Iron oxide nanotubes can be obtained by different methods such as solvothermal syntheses, biomacromolecules template, AAO template and electrochemical anodization [20–22]. Among them, electrochemical anodization method shows advantages of easily controllable pore size, good uniformity and conformability over large areas at low coat that is attractive for the formation of ordered nanochannel or nanotubular films onto the surface of valve metals [19]. Because of importance of this issue, the formation of iron oxide nanotubes with high surface area has been paid much interest by a number of researchers. Misra et al. [23] have first fabricated Fe_2O_3 nanotubes by sonoelectrochemical anodization method for water photo-oxidation. Grimes et al. [24] have discussed temperature dependent growth of Fe_2O_3 nanotubes by anodization method. However, to our best knowledge, there is no study directed toward the understanding between anodizing time of iron and the solar

light water splitting performance of the Fe_2O_3 nanotubes synthesized by the anodization technique. Therefore, it is of immense importance to understand this relationship in order to optimize the H_2 generation ability of the Fe_2O_3 nanotubes. In this work, Fe_2O_3 nanotube arrays were prepared from the electrochemical anodization of iron foils in a fluoride containing solution and their performance on the Photo-electrochemical (PEC) water splitting was investigated. Energy dispersive X-ray spectroscopy (EDX), X-ray diffraction (XRD) analysis and UV–vis diffuse reflectance spectra (DRS) were employed to get information on their structure and composition, while their morphology was studied by scanning electron microscopy (SEM). Here, we focused on the optimization of anodizing time of iron in synthesis of Fe_2O_3 nanotubes films for PEC water splitting. Furthermore, the amount of H_2 evolved during the illumination of the Fe_2O_3 nanotubes films will be measured to evaluate its solar energy conversion efficiency.

2 Experimental

2.1 Chemicals and solutions

All the reagents used in this synthesis were of analytical grade and used as received without further purification. All electrochemical experiments were carried out at room temperature. Distilled water was used throughout.

2.2 Fabrication of Fe_2O_3 nanotube arrays electrode

Pure iron foils with 1 mm thickness (purity: 99.9 % Fe) are used in the present study. The iron plates were first mechanically polished with emery papers (with the following grades: 80, 320, 800, 1,200, and 2,400), and then carefully rinsed, sequentially, in methanol, and distilled water. The anodization experiments were carried out using a two-electrode system with iron foil as anode and platinum with about 12 cm^2 geometric area foil as cathode, respectively. A controlled dc power source (ADAK, PS405) supplied the required constant voltage and a digital multimeter (Senit, DT-9208A) measured the anodization current. Anodization was carried out in an ethylene glycol electrolyte containing 0.1 M ammonium fluoride and 1 M H_2O water under a constant DC voltage of 40 V for different time at 25 °C. A schematic representation of the anodization setup is shown in Fig. 2. After anodization at a given reaction time, the samples was taken out of the solution, washed several times with distilled water, dried in air and then the samples were annealed in oxygen atmosphere at 450 °C for 1 h (2 °C/min) to convert the amorphous Fe_2O_3 to crystalline Fe_2O_3.
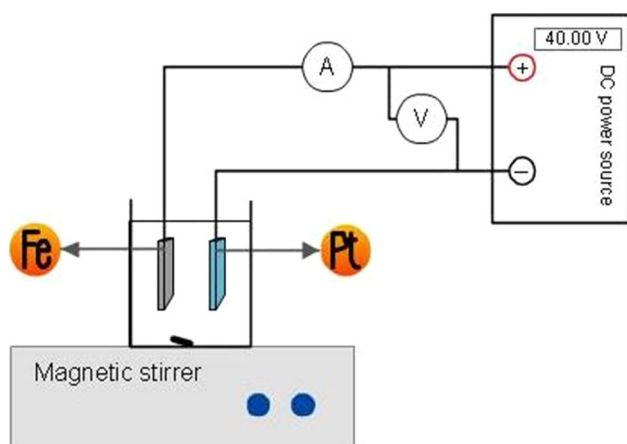
Fig. 2 Schematic diagram of the anodization set-up used to fabricate Fe_2O_3 nanotubes arrays

2.3 Characterization

The surface morphologies of all samples were characterized by field emission scanning electron microscopy (FE-SEM, Hitachi S-4160, Japan), and the elemental composition was estimated by energy dispersive X-ray spectroscopy (EDX). The crystalline phases were identified by XRD (Philips ́XPert). Diffraction patterns were recorded in the 2θ range from 20 to 80° at room temperature. UV–visible absorption spectra of the samples were recorded on a photospectrometer (JASCO V-570).

2.4 PEC water splitting

The PEC properties of the Fe_2O_3 nanotubes samples were performed using a Compactstat IviumStat (Model 2.175) with a three electrode configuration: a working electrode (Fe_2O_3 nanotubes/Fe), a platinum-wire counter electrode and an Ag/AgCl reference electrode. For photocurrent measurements, the electrodes were immersed in a solution of 1 M NaOH (pH 13.6). The hematite electrode was scanned from −300 to 500 mV (versus Ag/AgCl electrode) at a rate of 5 mV/s. Chronoamperometry was performed by measuring the current as a function of the time at 0.20 V (versus Ag/AgCl). The Fe_2O_3 nanotubes films were illuminated with a 200 W Xenon lamp equipped with a UV cut-off filter ($\lambda > 420$ nm). The luminous intensity of the Xenon lamp was 100 mW/cm^2. 100 % of the light was transmitted by the quartz glass as the xenon lamp shone on the Fe_2O_3 nanotubes (photo-anode). The xenon lamp was switched on after the three electrodes were connected to the potentiostat. Hydrogen evolution was measured for 1 h and H_2 gas was collected using the water displacement technique. As H_2 gas is produced at the counter-electrode in the PEC cell, it bubbles up into an inverted burette from which

the volume can be read. Figure 3 shows a schematic diagram of the experimental set-up for PEC water splitting.

3 Results and discussion

3.1 Anodization process of iron foil

Anodizing is an electrolytic process that creates a protective or decorative oxide film over a metallic surface. To accomplish it, the conducting piece undergoing anodizing is connected to the positive terminal of a dc power supply and placed in an electrolytic bath where it serves as the anode. The cathode is commonly a plate of platinum. When power is applied, electrons are forced from the electrolyte to the positive anode. The process leaves surface metal atoms exposed to oxygen ions within the electrolyte. The atoms react and become an in situ integral part of the oxide layer. The electrons travel through the power source and return to the cathode where and react with hydrogen ions and the combination bubbles off as hydrogen gas. Electrolytes having lower diffusion coefficients are known to prevent local acidification at the oxide-electrolyte interface. Hence in our studies ethylene glycol was used as the electrolytic medium. Fe_2O_3 nanotubes were obtained in an electrolyte consisting of 1 M H_2O + 0.1 M ammonium fluoride (NH_4F) in ethylene glycol under a constant voltage of 40 V for different time at 25 °C. Figure 4 shows the current–time behavior during the anodization. According to the Fig. 4, it can be said that in the anodization process, with an applied voltage of 40 V, the sharp drop of the current behavior in the first 30 s was due to the formation of initial oxide layer, followed by an increase in current due to the oxide layer pitting by the fluoride ions in the chemical dissolution process, and the current gradually increased. It was suggested that the formation of a passive film onto the iron surface upon anodizing anodization process in ethylene glycol solutions containing some fluorides and water proceeds via two reactions [25]:

1. Electrochemical oxidation: Iron oxidizes to form a thin layer of Fe_2O_3 on Fe metal at the solid–liquid interface by following equation:

$$2Fe + 3H_2O \rightarrow Fe_2O_{3(anodic)} + 3H_{2(cathodic)} \quad (3)$$
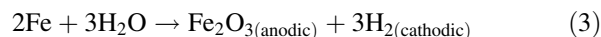
2. Chemical dissolution: Although Fe_2O_3 is thermodynamically stable in applied pH range, the presence of a complexing ligand (e.g., fluoride ion) and high applied potential leads to substantial dissolution of Fe_2O_3 by Eq. 4:

$$Fe_2O_3 + 12F^- + 6H^+ \rightarrow 2[FeF_6]^{3-} + 3H_2O \quad (4)$$
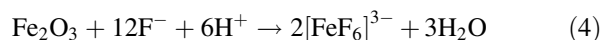
This complex formation leads to breakage in the oxide layer, with disordered pit formation followed by the formation of Fe_2O_3 nanotubes. This structure after further
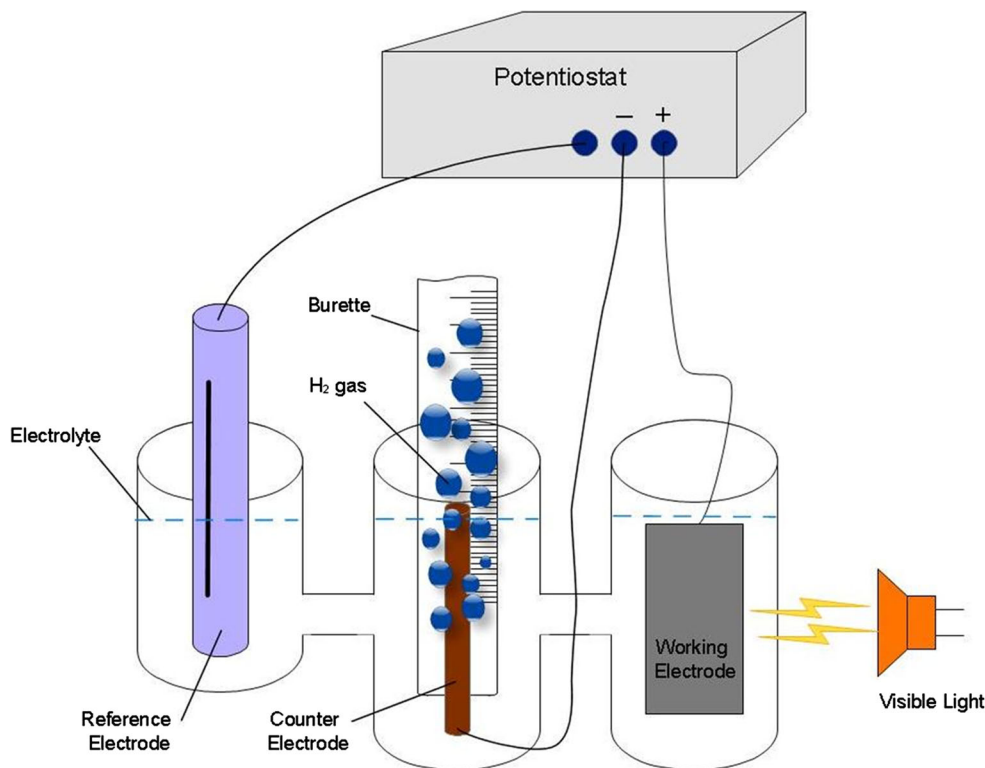
Fig. 3 Schematic diagram of the experimental set-up for PEC water splitting

dissolution forms self-standing individual nanotubes on the iron foil. The self-organized Fe_2O_3 nanotubes formed on the iron surface as a result of a combined effort as shown in Eqs. 3 (field-assisted) and 4 (field + chemical dissolution).

3.2 Morphology of Fe_2O_3 nanotubes

Morphology of the as-prepared Fe_2O_3 nanotubes along with reaction time was characterized by field-emission scanning electron microscopy. Fe_2O_3 nanotubes samples prepared by anodization of iron foil at a potential of 40 V in EG + 0.1 M NH_4F + 1 M distilled water at room temperature. From FE-SEM images the average pore size is measured to be approximately 39 nm for 60 min, 31 nm for 90 min and 43 nm for 120 min. By increase the time anodizing, the number of cracks increases. As shown in Fig. 5, by increasing anodizing time, we can observe that length of the nanotubes were increases. The analysis of the Fe_2O_3 nanotube samples surface by energy dispersive X-ray spectroscopy (EDX) taking measurements on top is shown in Fig. 6. The analysis revealed that the surface present similar composition with presence of Fe as a main energy E = 6.5 kV and O at E = 0.5 kV confirming that the iron oxide film was formed. The occurrence of contaminants such as carbon and fluorine from precursors are also observed.
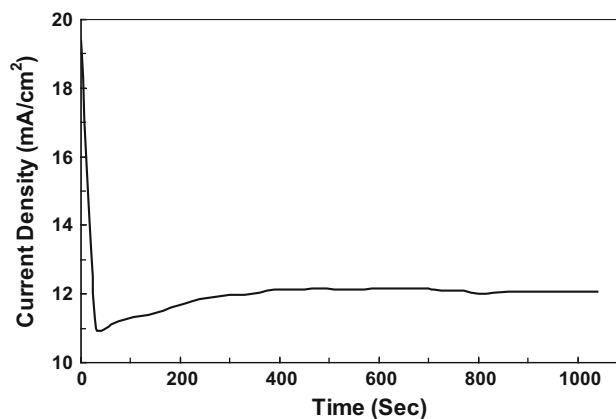

Fig. 4 Current transient during anodization of iron in aqueous ethylene glycol (0.1 M NH_4F and 1 M H_2O) solution at 40 V

3.3 Optical characterization

The optical properties such as absorption and optical band gap energy of Fe_2O_3 nanotube film are determined from the variation of absorption density. From the absorption data the band gap energy was calculated, according to solid band theory, using the following equation [26]:

$$(\alpha h\upsilon) = A\left(h\upsilon - E_g\right)^n \tag{5}$$
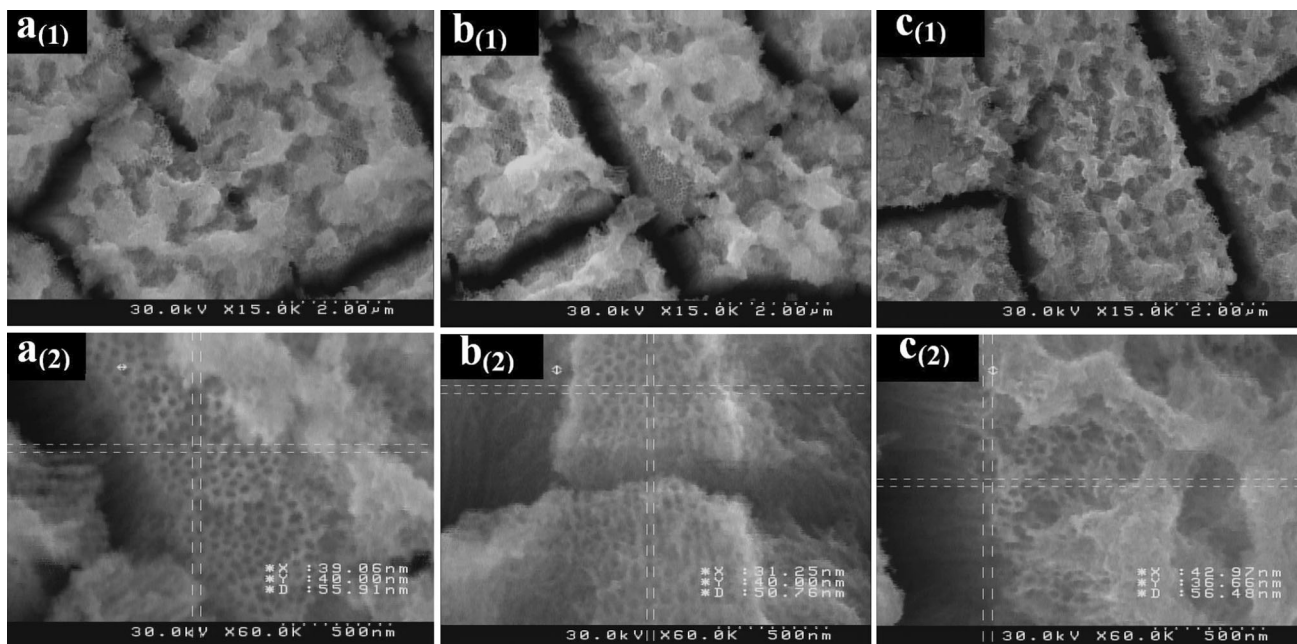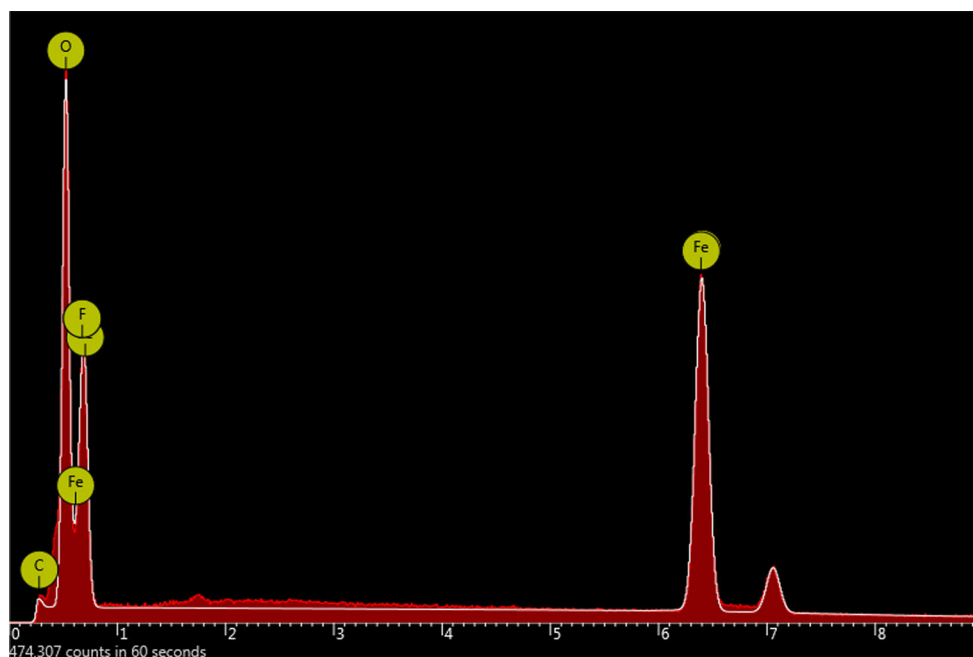
Fig. 5 SEM image the as-fabricated Fe_2O_3 sample grown from a 0.1 M NH_4F + 1 M distilled water in ethylene glycol for **a** 60 min, **b** 90 min and **c** 120 min at 40 V, with different magnifications

Fig. 6 Energy dispersive X-ray spectroscopy (EDX) analysis of Fe_2O_3 nanotubes grown on iron foil for 60 min

where E_g is the band gap energy, h is Planck's constant, υ is the frequency of vibration, $h\upsilon$ is the photon energy, A is a proportional constant and α is the absorption coefficient and n is 0.5 and 2.0 for a direct transition semiconductor and indirect transition semiconductor, respectively. Figure 7 shows optical absorption spectrum and plot of $(\alpha h\upsilon)^{1/2}$ against the energy of absorbed light. The maximum absorption wavelength was

around 344 nm, and the band gap absorption edge was around 567 nm. The absorption in the UV region corresponds to the direct charge transfer transitions of O^{2-} 2p $\rightarrow$ Fe^{3+} 3d, and the absorption in the visible region is due to the Fe^{3+} 3d $\rightarrow$ 3d indirect transition [19]. The band gap value is determined from the curves extrapolations and was found to be approximately the same for all the samples and is 2.04 eV.
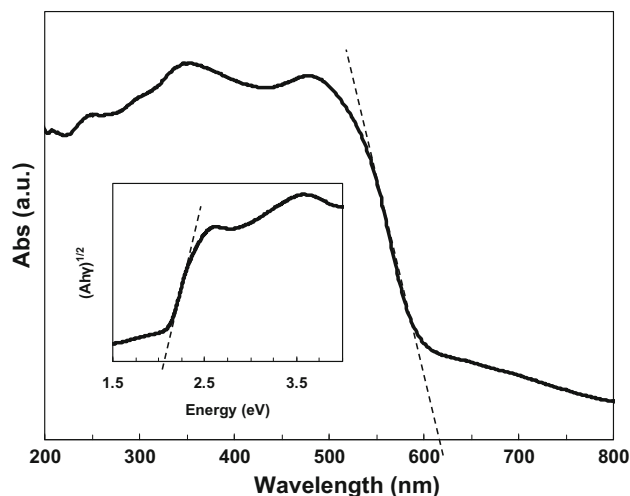
Fig. 7 UV-vis absorption spectra of the prepared Fe_2O_3 nanotube film (*inset* shows the Tauc plots calculated from the data)
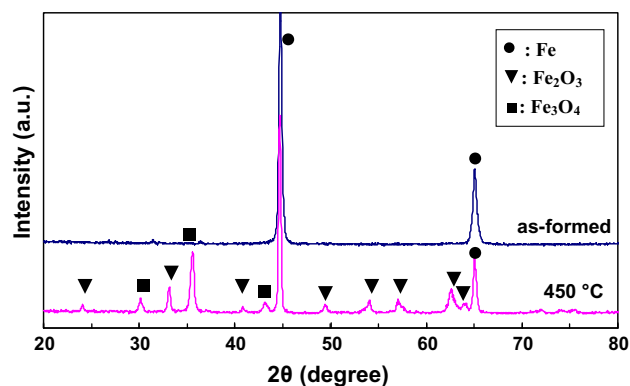

Fig. 8 XRD spectra from a self-organized nanoporous layer formed on Fe using 0.1 M NH_4F + 1 M distilled water in ethylene glycol for 60 min at 40 V before and after annealing

Fig. 9 Current versus potential curves of Fe_2O_3 nanotube photo-anodes prepared with different anodization time in the dark and under simulated solar light in a 1 M NaOH electrolyte solution

Fig. 10 H_2 evolution for Fe_2O_3 nanotube photo-anodes prepared with different anodization time

3.4 Structure of the Fe_2O_3 nanotubes

The crystal structure of the as-anodized and annealed iron oxide nanotube films were examined by X-ray diffraction (XRD) and Fig. 8 shows the corresponding XRD patterns. The as-anodized Fe_2O_3 nanotubes were amorphous in nature and no significant crystalline oxide structure was found. These nanotube were crystallized into α-Fe_2O_3 after annealing at 450 °C in oxygen atmosphere for 1 h. In addition, a very small amount of Fe_3O_4 (magnetite) is observed as the secondary phase, which is much less than that of α-Fe_2O_3.

3.5 Photo-electrochemical activity

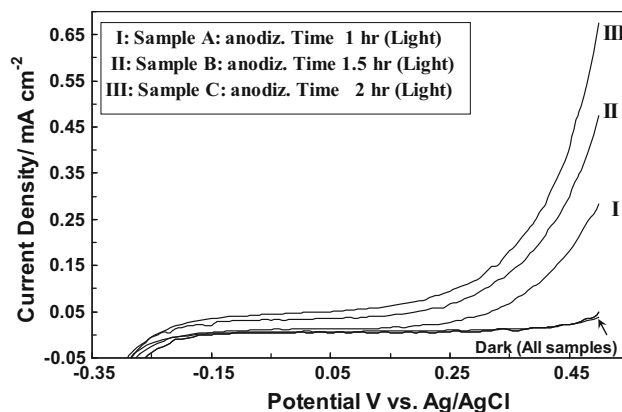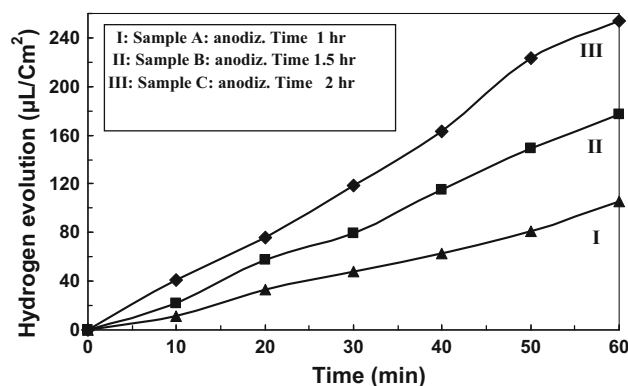Figure 9 shows the relation between applied potential and resultant current with and without illumination of the different samples that were annealed in the oxygen atmosphere at 450 °C for 1 h (2 °C/min). The I–V behavior is regarded as an indirect way to measure the rate of H_2 generation by water splitting if the Faradaic efficiency for water oxidation is assumed unity. The measured potentials vs. Ag/AgCl are converted to the reversible hydrogen electrode (RHE) scale according to the Nernst equation:

$$E_{RHE} = E_{Ag/AgCl} + 0.059pH + E^0_{Ag/AgCl} \qquad (6)$$

where E_{RHE} is the converted potential versus RHE, $E^0_{Ag/AgCl}$ = 0.197 V (25 °C), and $E_{Ag/AgCl}$ is the experimentally measured potential reference to Ag/AgCl electrode.

Under dark condition, all electrodes did not show any current generation either. The dark current remained low until the redox potential was reached for oxygen evolution in 1 M NaOH solution (0.2 V Ag/AgCl). Under light irradiation, photocurrent is observed over a region

Table 1 Comparison of the photocurrent density of the present study with similar studies

Electrodes	Electrolyte	Photocurrent density (mA/cm^2)	Ref.
α-Fe$_2$O$_3$	1 M NaOH	0.2 (at 0.4 V vs. Ag/AgCl)	[27]
α-Fe$_2$O$_3$	1 M KOH	0.2 (at 0.4 V vs. Ag/AgCl)	[13]
α-Fe$_2$O$_3$	1 M NaOH 1	0.72 (at 0.5 V vs. Ag/AgCl)	[28]
Ti-doped Fe$_2$O$_3$	M NaOH 1 M	0.103 (at 0.2 V vs. SCE)	[29]
Cd-Fe$_2$O$_3$	NaOH 1 M	1.1 (at 0.193 V vs. SCE)	[30]
ZnFe$_2$O$_4$	NaOH 1 M	0.35 (at 0.23 V vs. Ag/AgCl)	[31]
α-Fe$_2$O$_3$ nonotubes	NaOH	0.35 (at 0.23 V vs. Ag/AgCl)	This work

Saturated calomel electrode (SCE)

starting from -0.1 V versus Ag/AgCl for all three Fe$_2$O$_3$ electrodes. Compared with sample A (anodized in 1 h) with photocurrent of 0.02 mA/cm^2, sample B (anodized in 1.5 h) and C (anodized in 2 h) showed photocurrent increases by 0.059 and 0.086 mA/cm^2 at 0.23 V versus Ag/AgCl, respectively. This potential at pH 13.8 adopted for comparison corresponds to 1.23 V vs. RHE, which is the theoretical potential necessary for water oxidation. The photocurrent intensity increases with anodization time. It can be said that the induced photocurrent increased with increasing tube length of Fe$_2$O$_3$ nanotube. These facts imply that Fe$_2$O$_3$ nanotube with longer tube length provide the larger surface area and induce the higher induced photocurrent under illumination. Hydrogen generation over Fe$_2$O$_3$ nanotube samples obtained with anodizing time is shown in Fig. 10. The total mount of H$_2$ evolved on the sample C was 254 μL/cm^2 after 60 min, which is approximately 1.43 times higher than that on the sample B (177 μL/cm^2) and 2.4 times higher than that on the sample A (106 μL/cm^2). These results are approximately in agreement with the photocurrent density results. In this study, the maximum photocurrent density was 0.68 mA/cm^2 at 0.5 V versus Ag/AgCl (for sample C). A comparison of the photocurrent density of the present study with similar studies is presented in Table 1.

One important feature of the catalyst to reduce the cost of the process is its ability to be reused. Figure 11 shows the hydrogen production of Fe$_2$O$_3$ nanotube photo-anode (sample C) as a function of sequence of reaction time, the hydrogen production volume has no obvious decay and maintains an average value of 240 μL/cm^2 after ten continuous running (60 min per running), which indicates that the Fe$_2$O$_3$ nanotube photo-anode have good mechanical strength and chemical stability in the water splitting process and could be a promising material for long-term hydrogen production. So we expect that this nanotube photo-anode will offer promising applications for renewable energy generation, environmental protection and other photoelectrochemical applications.
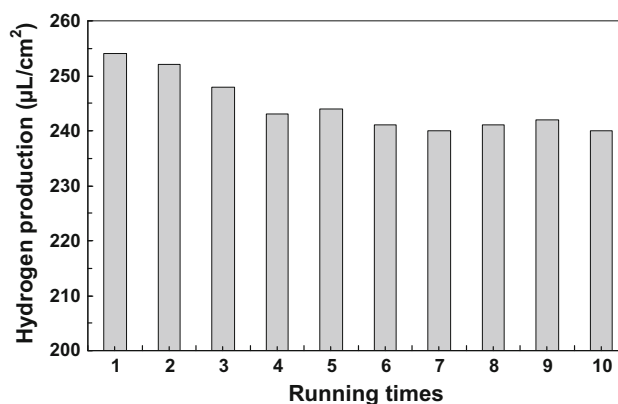

Fig. 11 H$_2$ evolution for Fe$_2$O$_3$ nanotube photo-anode (sample C) as a function of running times

4 Conclusions

Pure iron samples were anodized at room temperature in an ethylene glycol electrolyte containing 0.1 M ammonium fluoride and 1 M H$_2$O water under a constant voltage of 40 V for different time. Annealing in an oxygen atmosphere at 450 °C for 1 h resulted in a predominantly crystallized nanoporous Fe$_2$O$_3$ film. XRD, SEM, EDX and UV–vis absorbance spectra have been used to characterize the Fe$_2$O$_3$ nanostructures. The pore size of the film can be controlled by adjusting the anodizing time. The optical and photo-electrochemical properties have been investigated. The results show that the band gap value of Fe$_2$O$_3$ films is 2.04 eV. The maximum photocurrent density is 0.68 mA cm^{-2} with a bias voltage of 0.5 V (V vs. Ag/AgCl), under a 200 W xenon lamp system.

References

1. A. Fujishima, K. Honda, Nature **238**, 37 (1972)
2. S.C. Moon, H. Mametsuka, S. Tabata, E. Suzuki, Catal. Today **58**, 125 (2000)

3. R. Liu, Y. Lin, L.Y. Chou, S.W. Sheehan, W. He, F. Zhang, Angew. Chem. Int. Ed. **50**, 499 (2011)
4. N. Chouhan, C.L. Yeh, S.F. Hu, R.S. Liu, W.S. Chang, K.H. Chen, Chem. Commun. **47**, 3493 (2011)
5. Y.H. Ng, A. Iwase, A. Kudo, R. Amal, J. Phys. Chem. Lett. **1**, 2607 (2010)
6. P. Chatchai, Y. Murakami, S.Y. Kishioka, A.Y. Nosaka, Y. Nosaka, Electrochim. Acta **54**, 1147 (2009)
7. R. van de Krol, Y. Liang, J. Schoonman, J. Mater. Chem. **18**, 2311 (2008)
8. J. Hensel, G. Wang, Y. Li, J.Z. Zhang, Nano Lett. **10**, 478 (2010)
9. G. Rahman, O.S. Joo, Int. J. Hydrogen Energy **37**, 13989 (2012)
10. A. Kay, I. Cesar, M. Grätzel, J. Am. Chem. Soc. **128**, 15714 (2006)
11. E.L. Miller, D. Paluselli, B. Marsen, R.E. Rocheleau, Sol. Energ. Mat. Sol. C. **88**, 131 (2005)
12. C.J. Sartoretti, B.D. Alexander, R. Solarska, W.A. Rutkowska, J. Augustynski, R. Cerny, J. Phys. Chem. B. **109**, 13685 (2005)
13. V.M. Aroutiounian, V.M. Arakelyan, G.E. Shahnazaryan, G.M. Stepanyan, E.A. Khachaturyan, H. Wang, Sol. Energy **80**, 1098 (2006)
14. Y. Liu, D.P. Wang, Y.X. Yu, W.D. Zhang, Int. J. Hydrogen Energy **37**, 9566 (2012)
15. C.Y. Lee, L. Wang, Y. Kado, R. Kirchgeorg, P. Schmuki, Electrochem. Commun. **34**, 308 (2013)
16. K. Sivula, F. Le Formal, M. Grätzel, Chem. Sun. Chem. **4**, 432 (2011)
17. L. Wang, C.Y. Lee, P. Schmuki, J. Mater. Chem. A. **1**, 212 (2013)
18. S. Grigorescu, C.Y. Lee, K. Lee, S. Albu, I. Paramasivam, I. Demetrescu, P. Schmuki, Electrochem. Commun. **23**, 59 (2012)
19. Z. Zhang, M.F. Hossain, T. Takahashi, Appl Catal B: Environ. **95**, 423 (2010)
20. D.D. Archibald, S. Mann, Nature **364**, 430 (1993)
21. J. Chen, L. Xu, W. Li, X. Gou, Adv. Mater. **17**, 582 (2005)
22. H.E. Parkasam, O.K. Varghese, M. Paulose, G.K. Mor, C.A. Grimes, Nanotechnology. **17**, 4285 (2006)
23. S.K. Mohapatra, S.E. John, S. Banerjee, M. Misra, Chem. Mater. **21**, 3048 (2009)
24. T.J. LaTempa, X.J. Feng, M. Paulose, C.A. Grimes, J. Phys. Chem. C **113**, 16293 (2009)
25. C.Y. Chang, C.H. Wang, C.J. Tseng, K.W. Cheng, L.W. Hourng, B.T. Tsai, Int. J. Hydrogen Energy **37**, 13616 (2012)
26. A. Elshabini-Raid, F. Barlow, *Thin Film Technology Handbook* (McGraw- Hill, New York, 1998)
27. J.Y. Kim, H. Jun, S.J. Hong, H.G. Kim, J.S. Lee, Int. J. Hydrogen Energy **36**, 9462 (2011)
28. C.S. Enache, Y.Q. Liang, R. van de Krol, Thin Solid Films **520**, 1034 (2011)
29. X. Lian, X. Yang, S. Liu, Y. Xu, C. Jiang, J. Chen, Appl. Surf. Sci. **258**, 2307 (2012)
30. A. Bak, W. Choi, H. Park, Appl. Catal. B: Environ. **110**, 207 (2011)
31. A.A. Tahir, K.G.U. Wijayanth, J. Photoch. Photobio. A **216**, 119 (2010)